Atmospheric Environment 309 (2023) 119927

Contents lists available at ScienceDirect

Atmospheric Environment

journal homepage: www.elsevier.com/locate/atmosenv

Rare Earth Elements' particles in road dust: A mineralogical perspective for source identification

Dídac Navarro-Ciurana [a,b,*], Mercè Corbella [a], Júlia Farré-de-Pablo [c], Isaac Corral [a], Elisabeth Buixadera [a], Robert Morera-Valverde [a], Joaquín A. Proenza [c]

[a] Departament de Geologia, Facultat de Ciències, Universitat Autònoma de Barcelona (UAB), Edifici Cs s/n, 08193, Bellaterra, Cerdanyola del Vallès, Spain
[b] Grup MAiMA, SGR Mineralogia Aplicada, Geoquímica i Hidrogeologia, Departament de Mineralogia, Petrologia i Geologia Aplicada, Facultat de Ciències de la Terra, i Institut de Recerca de l'Aigua (IdRA), Universitat de Barcelona (UB), c/ Martí i Franquès s/n, 08028, Barcelona, Spain
[c] Departament de Mineralogia, Petrologia i Geologia Aplicada, Facultat de Ciències de la Terra, Universitat de Barcelona (UB), c/ Martí i Franquès s/n, 08028, Barcelona, Spain

HIGHLIGHTS

- CeO_2 crystals from road dust are identified as discrete micro- and nano-particles.
- Inhalable CeO_2 particles are emitted to the environment by autocatalytic converters.
- Neo-formed CeO_2 occurs by CeO_2–ZrO_2 phase segregation from the catalyzer washcoat.
- The mineralogical study of road dust' particles is a powerful source tracer tool.

GRAPHICAL ABSTRACT

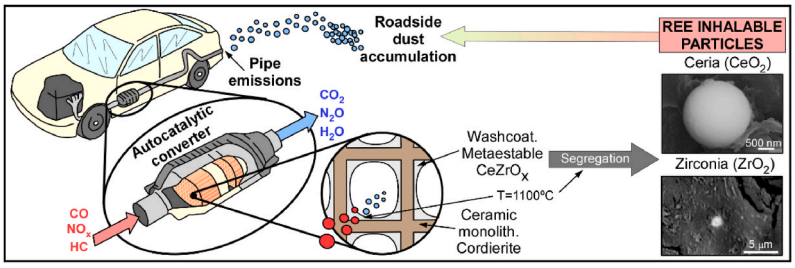

ARTICLE INFO

Keywords:
REE mineralogy
Ceria nano-particles
Autocatalyst
Vehicle emissions
Anthropogenic inhalable particles

ABSTRACT

Roadside dust contains many mineral grains and, among them, some of REEs (Rare Earth Elements) which have an uncertain origin. This paper characterizes and illustrates for the first time the occurrence of such REEs' particles from four locations near Barcelona (Spain), by means of mineralogical studies, with the aim of identifying their source and understanding their accumulation. The observed REEs' particles contain Ce and low amounts of La and Nd and are spheroidal, rounded, elongated, or angularly shaped (<5 μm), often forming nanoparticles' aggregates. The identical chemical composition and morphology of the REEs' particles (CeO_2), independently from the sampling location and its geological background, points to a sole non-natural anthropogenic origin. Moreover, the absence of U and Th in the studied CeO_2 grains is an additional robust indicator of their anthropogenic source, as the naturally formed CeO_2 (the mineral cerianite) is characterized by containing those radioactive elements. Therefore, the identified grains consist of ceria particles, the non-natural cerium oxide. Ceria must originate in autocatalytic converters, where it is broadly used in solid solution with ZrO_2 (zirconia) in the form of $CeZrO_x$. The roadside dust ceria particles do not contain Zr, but zirconia crystals are also found in the dust, with no Ce traces. This might indicate that they were released as separated neo-formed ceria and zirconia phases, which is consistent with a metastable $CeZrO_x$ segregation at the autocatalyzer under vehicles' engine operating conditions. The small size, and thus inhalable, ceria particles emitted by vehicles are a

* Corresponding author. Departament de Geologia, Facultat de Ciències, Universitat Autònoma de Barcelona (UAB), Edifici Cs s/n, 08193, Bellaterra, Cerdanyola del Vallès, Spain.
E-mail address: didac.navarro@uab.cat (D. Navarro-Ciurana).

https://doi.org/10.1016/j.atmosenv.2023.119927
Received 12 April 2023; Received in revised form 14 June 2023; Accepted 25 June 2023
Available online 30 June 2023

significant environmental health hazard, revealing the need for further assessment of CeO_2 concentrations generated by automobiles in urban areas worldwide.

1. Introduction

Ambient particulate matter (PM) pollution, which can be accumulated on urban roads, is one of the global modern society challenges (WHO, 2016). Road dust is constituted by different fractions of geogenic and anthropogenic particles, which commonly act as a toxic PM temporary storage (Haynes et al., 2020, and references therein). The particles of geologic origin come from the rock and soil erosion of a specific location so that they reflect their composition. Therefore, areas with different rock formations would provide different type of particles such as carbonates, silicates, sulfides, sulfates, and oxides. If the geology of an area is well-known, the PM mineralogy can be traced back to particular rocks. Minerals of Rare Earth Elements (REEs) may be found as minor or trace components in igneous, sedimentary or metamorphic rocks (Chakhmouradian and Wall, 2012).

On the other hand, the anthropogenic particles may originate in industries, automobiles, construction sites, etc. It has been widely documented that a potential road dust's PM source is the automotive three-way catalytic converters (TWCCs) abrasion and ware (e.g., Bozlaker and Chellam, 2015; Chellam and Bozlaker, 2015; Clement et al., 2015; Wiseman et al., 2016; Meza-Figueroa et al., 2021; Navarro-Espinoza et al., 2022). TWCCs convert the unburned hydrocarbons, CO and NO_x pollutants into less harmless exhaust gas by redox reactions in the presence of Platinum Group Elements (PGEs: Dey and Mehta, 2020; Yoshida et al., 2022). This automotive emission control device contains a honeycomb-type cordierite monolith ($Mg_2Al_4Si_5O_{18}$), which is coated with a thin layer of active catalysts nanoparticles. They are made of PGEs and a thermodynamically metastable ceria (CeO_2) and zirconia (ZrO_2) solid solution, commonly in the form of $Ce_xZr_{1-x}O_2$ (Heck and Farrauto, 2001; Navarro-Espinoza et al., 2022). It is used to promote oxygen storage, release capacity and thermal stability of TWCCs (Trovarelli, 1996; Reddy and Khan, 2005).

Although some research provides evidences that REEs on urban dust, particularly Ce and La, are anthropogenically sourced from TWCCs (Varrica et al., 2003; Wiseman et al., 2016; Meza-Figueroa et al., 2021), there is still some uncertainty about their potential geogenic origin (e.g., Dehghani et al., 2018). This is partially related with the fact that environmental studies on road dust are routinely focused on the REEs bulk composition, overlooking the mineralogical features of particles. For instance, Haynes et al. (2020) recommended supplementing urban dust' bulk chemical data with accurate mineralogical characterization of grains to infer their sources, mobility, fate and environmental risk.

To the best of the authors knowledge, there are no accurate studies on the mineralogical characterization of road dust' ceria particles. Meza-Figueroa et al. (2021) characterized the zirconia, ceria and $CeZrO_x$ crystallinity in automobile converters and exhaust pipes from vehicles and road dust with powder X-Ray Diffraction (XRD). They also observed zirconia crystals on road dust under a scanning electron microscope equipped with an energy-dispersive spectrometer (SEM-EDS) but did not report the mineralogical study of the ceria particles. The low total REE contents in the road dust and the very small grain size of the particles challenges the identification and characterization of ceria and similarly small particles.

In this work, a detailed mineralogical characterization of road dust' particles, with emphasis on the heavy metals and REEs, is carried out on the Barcelona urban area (NE Iberian Peninsula) with the aim of identifying their source. Barcelona has one of the highest vehicle densities in Europe and is one of the most polluted cities in Western Europe (EEA, 2019). Moreover, from a geological point of view, Barcelona sits on a great diversity of lithologies of different nature and age (Fig. 1). Therefore, this setting provides an excellent opportunity to elucidate the geogenic or anthropogenic origin of road dust' particles and to understand their accumulating mechanism in the environment. A review of worldwide road dust's bulk chemical composition has also been conducted to illustrate the advantages and limitations when used as a discrimination tool for REEs' particle sources.

2. Materials and methods

2.1. Geographical and geological context of the study area

The study was carried out in the Barcelona Province (Catalonia), located in the NE of the Iberian Peninsula, with the sampling sites located in the city of Barcelona and in the adjacent municipalities of

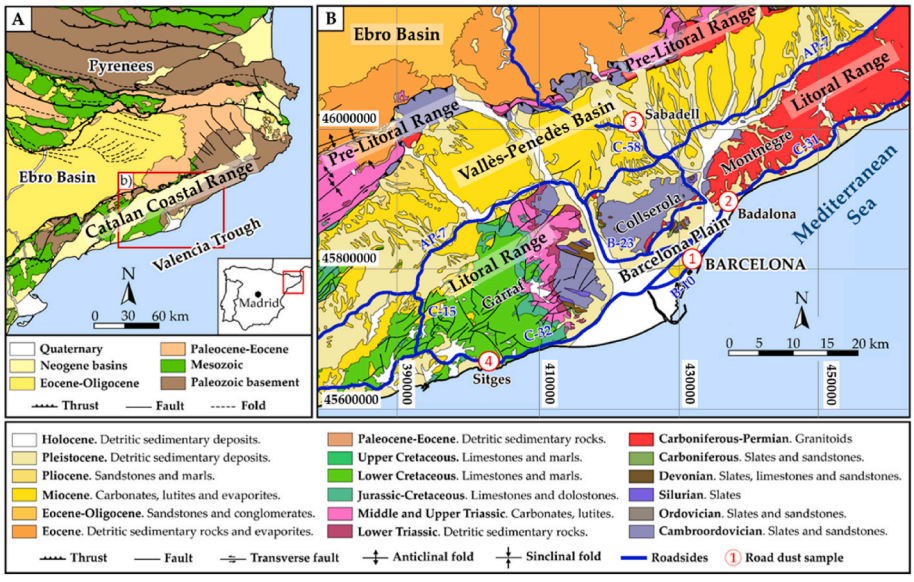

Fig. 1. A) Regional geologic map of Catalonia (Spain) with the location of the Catalan Coastal Ranges and the study area (modified from Guimerà et al., 2004). **B)** Location of sampling sites on a geologic map of the Barcelona Province (Spain; modified from ICGC, 2019).

Badalona, Sabadell and Sitges (Fig. 1). From the geological point of view, the study area is ubicated in the Catalan Coastal Ranges (CCR) which extend 200 km between the Ebro Basin (Pyrenees foreland basin) and the Valencia Through (Fig. 1a). The CCR are formed by two parallel mountain ranges, the Pre-Litoral and Litoral Ranges, which are separated by the Vallès-Penedès Basin (Fig. 1b: Anadón et al., 1985; Guimerà, 1983; Guimerà et al., 2004). In addition, the CCR is delimited to the E by a series of normal faults with widespread dip towards SE separating it from the Barcelona Plain (Fig. 1: Gómez and Guimerà, 1999). Furthermore, the CCR consists of 4 large groups of differentiated geological units (Anadón et al., 1979): i) Hercynian basement, mainly characterized by metasedimentary rocks of Cambrian-Ordovician to Permian age, as well as granitic intrusions that crop out extensively in both ranges; ii) Mesozoic cover, constituted by Triassic materials and mainly carbonated rocks of Jurassic and Cretaceous age, found broadly in the Litoral Range; iii) Paleogene materials of marine and continental origin mainly outcropping in the Vallès-Penedès Basin; and iv) Neogene and Quaternary sedimentary deposits located in the depressions originated during the Miocene distension (e.g., Vallès-Penedès and Barcelona Plain). Additional geological features of the study area may be found in Anadón et al. (1979) and Santanach et al. (2011).

Barcelona constitutes one of the European cities with the highest vehicle density (6.100 vehicles·km^{-2}; Reche et al., 2011) and the second most densely populated city of Spain (16.420 inhabitants km^{-2}; IDESCAT, 2019). Badalona, a city geographically adhered to Barcelona, has also high traffic-clogged urban areas and a high-density population (10.537 inhabitants·km^{-2}; IDESCAT, 2019). In both city centers, the predominance of narrow streets and a dearth of green areas hinder the dispersion of pollutants. On the other hand, Sabadell lies in the Vallès-Penedès Basin 15 km away from the coast (Fig. 1b). The city of Sabadell, which shows a density population of around 5.730 inhabitants·km^{-2} (IDESCAT, 2019), has an important industrial development, with a large transport infrastructure involving trains, light railway, and abundant road traffic. Finally, Sitges, a popular touristic destination, is a Mediterranean town with scarce industry located in the southern part of the Litoral Range (Fig. 1b). Although Sitges has around 30,000 inhabitants (IDESCAT, 2019), during the summer season the population number doubles.

2.2. Sample sites and sampling descriptions

The sampling sites were strategically selected considering the main lithologies outcropping in the Barcelona area (Fig. 1) and roads with low-to high-traffic density to illustrate the potential of mineralogical studies to identify road dust REEs' sources. Sampling was performed in all localities (Barcelona, Badalona, Sabadell and Sitges) on January 13th' 2019, after 15 dry days. Approximately 24 kg of composite road dust, ~6 kg for each selected site, were collected using a plastic bristle brush and dustpan and stored in plastic bags.

The samples were obtained sweeping off (Fig. 2 and Table 1): i) the curb and median strip of the Barcelona Colon Street (200 m^2 swept; Sample 1), which run parallel to the second busiest road of the city (B-10 highway; avg. 110,000 vehicles per day); ii) the southern shoulder road and a clogged sewer disposed on a concrete gutter of the Badalona Guixeres Street (160 m^2 swept; Sample 2), a low-traffic road that runs parallel to the C-31 dual carriageway access road to Barcelona (avg. 70,000 vehicles per day); iii) 97 m of an asphalt gutter located in the median strip of the C-58 dual carriageway (150 m^2 swept; Sample 3), that corresponds to the principal access road of Sabadell city (44,000 vehicles circulating daily); and iv) the shoulder road and a concrete gutter on the northern margin of the C-32 toll motorway (150 m^2 swept; Sample 4; 30,000 vehicles per day), which is located in the Sitges municipality and near a cement plant and a waste landfill of 67 ha^2.

Road dust at Colon Street is considered a representative of anthropogenic origin due to the absence of nearby geological outcrops (Fig. 2a). However, a contribution from the surrounding Paleozoic and Cenozoic mountains cannot be discarded (Fig. 1). It is worth noting that in the northern sector of the Badalona Guixeries Street a Pleistocene red clay crops out (Fig. 2b), which must contribute with natural sediments to the sampled composite, as reddish particulate matter was visually identified. Nevertheless, weathered Paleozoic granitoids nearby may also contribute (Fig. 2). Field geological observations conducted at C-58 dual carriageway of Sabadell confirmed the existence of Pleistocene sandstone outcrops, which can contribute with geogenic particles to the sampled road dust (Fig. 2). Finally, the main lithologies that could add particles to road dust sampled at C-32 toll motorway of Sitges are Lower to Upper Cretaceous carbonates, that extensively outcrop in the studied area (Figs. 1 and 2).

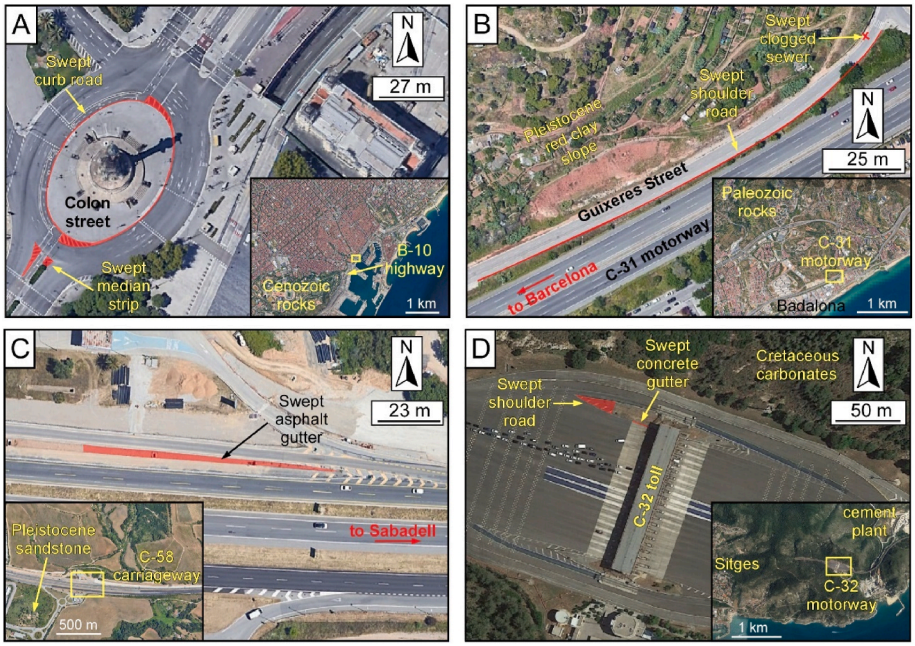

Fig. 2. Location of sampling sites. **A)** Barcelona Colon Street. **B)** Badalona Guixeres Street. **C)** Sabadell C-58 dual carriageway. **D)** Sitges C-32 toll motorway.

Table 1
Samples and sampling sites.

Site/ sample	Geographical coordinates (WGS84, UTM zone 31)		Elevation (m above sea level)	Road location	Traffic (vehicle per day)	Sample location	Road swept (m^2)	Sample weight (g)
	Easting	Northing						
1	431,221	4,580,765	4	Colon square (Barcelona)	110,000	Curb, median strip	200	5750
2	438,857	4,590,495	130	C-31 dual carriageway (Badalona)	Low-traffic	Shoulder, clogged sewer	160	6301
3	420,902	4,599,424	928	C-58 dual carriageway (Sabadell)	44,000	Gutter in median strip	150	6110
4	403,791	4,566,653	62	C-32 freeway (Sitges)	30,000	Shoulder and gutter	150	5906

2.3. Sample preparation

All samples were initially dry-sieved using disposable 125 μm size meshes to remove extraneous matter, such as leaf litter, asphalt particles, small pieces of brick, glasses, plastics or concrete and any other debris. Subsequently, wet sieving at 125 μm was performed with deionized water to fruitfully dislodge the fine particles from the coarser ones. After this process, around 1.5 kg of dust with <125 μm fraction size were obtained for each sample. The samples were dried under ambient conditions, and then homogenized and quartered into different subsets of 150–300 g to conduct the current study. For the mineralogical study, representative fractions of each sample were embedded as a thin "layer" in 5 cylindrical (d = 2.5 cm) epoxy-resin mounts (hereafter called monolayers).

In order to ensure finding the very small sized REEs' particles, one of the roadside dust samples (Sample 4; Table 1) was processed for concentrating dense particles applying the hydroseparation (HS) technique (Aiglsperger et al., 2015) at the Hydroseparation laboratory of the University of Barcelona (Fig. 3). This technique allows the concentration of heavy particles from different size fractions (particles as small as <30 μm) by using water instead of other dense liquid separation methods, also avoiding the contamination of the sample.

The HS methodology simulates natural beach placer deposits by a combination of laminar water flow at constant pressure with diverse wave impulses. Dense mineral phases (e.g., sulfides, REEs' particles or zircons, among others) are collected at the bottom of a so-called glass separation tube (GST), whereas light particles (e.g., quartz, feldspar, micas, etc.) rise to the top of the GST and leave the system (Fig. 3). Using different GSTs, flow rates, and impulse regimes, the total amount of final heavy mineral concentrates is reduced to about 10 mg. However, to ensure that the different particles are really separated by density, the sample must have similar fraction size. Therefore, for this process, all the obtained <125 μm fraction was further dry- and wet-sieved using mesh sizes of 75 μm and 30 μm, applying the process described above. As a result, three different fractions were obtained (75–125 μm, 30–75 μm and <30 μm) which were treated using the computer-controlled Hydroseparation device CNT HS-11 (Cabri et al., 2008, Fig. 3) applying the methodology for soft rocks described in Aiglsperger et al. (2015, and references therein). The densest grains separated by means of HS were embedded in monolayers.

After sieving and HS application a total of 26 monolayers (5 for each sieved sample at < 125 μm fraction and two for each fraction treated using HS) were obtained for further mineralogical analysis. They were metallographically polished using a monocrystalline shape edges diamond abrasive paste of 1 μm, an ultrasonic bath was used to remove any remaining polishing material from the sample. A control dust sample

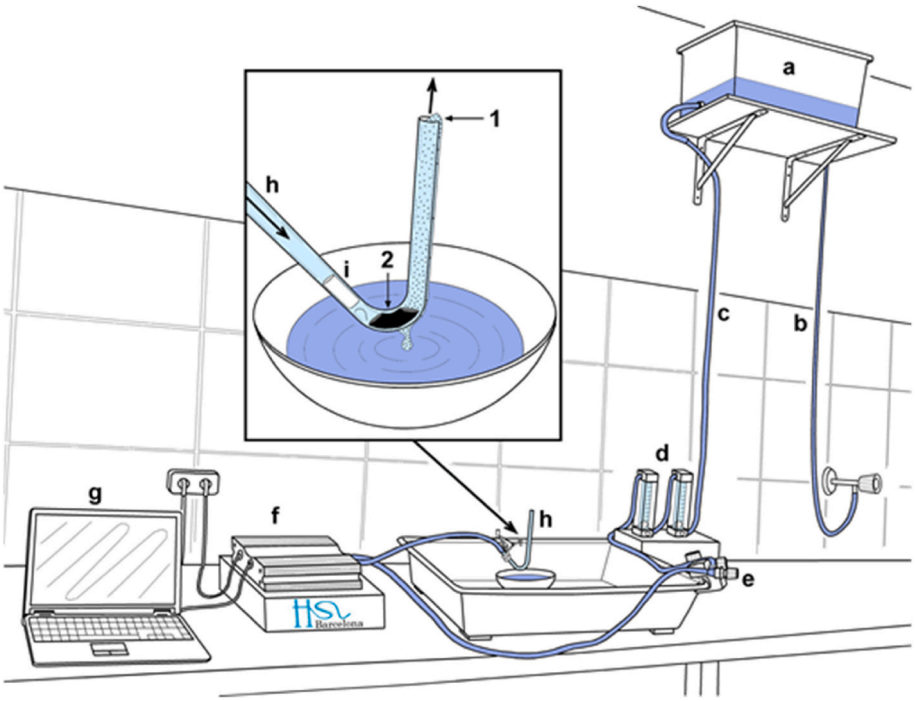

Fig. 3. Scheme of the HS-11 laboratory. The HS-11 is composed of a) an elevated water tank; b) a silicone tube connected to conventional stream; c) a silicone tube connected to a flowmeter; d) a flowmeter; e) a stopcock; f) the HS-11device; g) a computer with the operating software CNT–HS–11; h) a glass separation tube (GST); and i) a glass cylinder. Lighter particles rise up (1), whereas heavy mineral grains are concentrated on the GST curvature (2).

from Sitges was mounted directly on a pin stub to compare the dust with that of the polished mounts and exclude possible contamination by the abrasive paste.

2.4. Scanning electron microscopy (SEM-EDS and FE-SEM-EDS)

The morphological and textural features and the semi-quantitative composition of particles in the roadside dust samples embedded in monolayers were examined at the Servei de Microscòpia of Universitat Autònoma de Barcelona (UAB) by means of scanning electron microscopy (SEM), using an environmental SEM EVO MA 10 5 (Zeiss, Jena, Germany) equipped with an energy dispersive spectrometer (EDS). The effectiveness of SEM-EDS is limited as the particles of interest occur in small sizes (around 1 μm). To overcome this, we carried out a more detailed study of mineral phases to determine their textural and qualitative compositional features with a Zeiss Merlin (Zeiss, Jena, Germany) field emission scanning electron microscope (FE-SEM). The operating conditions in both cases were an accelerating voltage of 20 kV and a beam current of 1 nA with a mean count time of 30s for analysis.

3. Results and discussion

3.1. Mineralogical characterization

3.1.1. REE's particles

43 particles with REEs were mineralogically investigated under FE-SEM-EDS on monolayer mounts, some from non-concentrated samples of <125 μm diameter (n = 17) and the rest from HS concentrated samples with particles of <30 μm size (n = 26) (Table 2). Although the studied REE's particles diameter range from 0.4 to 5.8 μm, 59% of them were comprised between 1.0 and 2.9 μm (Table 2 and Fig. 4). Half of the REE's grains were identified as isolated particles, whereas the other half were adhered to other mineral surfaces (i.e., silicates, carbonates, Fe-oxi-hydroxides, metallic elements and alloys). It should be noted that no inclusions of REEs were observed within other particles.

Additionally, a REEs' particle was identified on the control dust sample mounted directly in a pin stub (Fig. 5a). This particle shows the same mineralogical features than the others found on the monolayers from the concentrated sample (Table 2 and Fig. 5a). Furthermore, a thin layer of the mounting resin could be observed by means of FE-SEM in

Table 2
Mineralogical characteristics of Barcelona's area road dust REE's particles.

Particle Nº	Site	Type of sample	Spatial occurrence	Type of particle	Size (nm)	Morphology	Chemical compound
1	Barcelona	Non-concentrated	Adhered	Monocrystalline	3196	Roundish	Ce, La
2	Barcelona	Non-concentrated	Adhered	Monocrystalline	3631	Edgy	Ce, La
3	Barcelona	Non-concentrated	Adhered	Aggregate	3119	Elongated	Ce, La, Nd
4	Barcelona	Non-concentrated	Adhered	Aggregate	3059	Elongated	Ce, La
5	Badalona	Non-concentrated	Adhered	Monocrystalline	1014	Roundish	Ce, Nd
6	Badalona	Non-concentrated	Adhered	Aggregate	830	Edgy	Ce, Nd
7	Badalona	Non-concentrated	Isolated	Monocrystalline	964	Spheric	Ce, La
8	Badalona	Non-concentrated	Isolated	Aggregate	3341	Roundish	Ce, La, Nd
9	Sabadell	Non-concentrated	Adhered	Monocrystalline	3413	Elongated	Ce, La, Nd
10	Sabadell	Non-concentrated	Isolated	Aggregate	2216	Elongated	Ce, La
11	Sabadell	Non-concentrated	Isolated	Aggregate	1308	Roundish	Ce, La
12	Sabadell	Non-concentrated	Isolated	Monocrystalline	4745	Edgy	Ce, La
13	Sabadell	Non-concentrated	Adhered	Monocrystalline	3636	Spheric	Ce, La
14	Sitges	Non-concentrated	Adhered	Monocrystalline	2054	Spheric	Ce
15	Sitges	Non-concentrated	Adhered	Aggregate	2821	Roundish	Ce, La
16	Sitges	Non-concentrated	Isolated	Aggregate	5848	Elongated	Ce, La, Nd
17	Sitges	Non-concentrated	Adhered	Monocrystalline	544	Edgy	Ce, La
18	Sitges	HS concentrated	Isolated	Monocrystalline	2076	Edgy	Ce, La
19	Sitges	HS concentrated	Adhered	Monocrystalline	1912	Spheric	Ce
20	Sitges	HS concentrated	Isolated	Monocrystalline	4481	Edgy	Ce, La
21	Sitges	HS concentrated	Adhered	Aggregate	875	Roundish	Ce, La
22	Sitges	HS concentrated	Adhered	Aggregate	2562	Roundish	Ce, La, Nd
23	Sitges	HS concentrated	Isolated	Aggregate	1784	Elongated	Ce, La
24	Sitges	HS concentrated	Adhered	Monocrystalline	4103	Spheric	Ce
25	Sitges	HS concentrated	Isolated	Monocrystalline	892	Edgy	Ce, La
26	Sitges	HS concentrated	Adhered	Aggregate	2782	Edgy	Ce, La
27	Sitges	HS concentrated	Isolated	Monocrystalline	1352	Spheric	Ce
28	Sitges	HS concentrated	Adhered	Monocrystalline	673	Edgy	Ce, La
29	Sitges	HS concentrated	Adhered	Monocrystalline	1123	Spheric	Ce
30	Sitges	HS concentrated	Isolated	Aggregate	1590	Elongated	Ce, La, Nd
31	Sitges	HS concentrated	Adhered	Monocrystalline	1647	Spheric	Ce
32	Sitges	HS concentrated	Isolated	Monocrystalline	1127	Elongated	Ce, La
33	Sitges	HS concentrated	Adhered	Monocrystalline	1615	Spheric	Ce
34	Sitges	HS concentrated	Adhered	Aggregate	1402	Roundish	Ce
35	Sitges	HS concentrated	Isolated	Monocrystalline	421	Spheric	Ce, La
36	Sitges	HS concentrated	Isolated	Monocrystalline	2079	Rounded	Ce, La
37	Sitges	HS concentrated	Isolated	Monocrystalline	1216	Edgy	Ce
38	Sitges	HS concentrated	Isolated	Aggregate	562	Roundish	Ce, La
39	Sitges	HS concentrated	Adhered	Aggregate	2102	Elongated	Ce, La
40	Sitges	HS concentrated	Isolated	Monocrystalline	2404	Edgy	Ce, La
41	Sitges	HS concentrated	Isolated	Aggregate	1540	Elongated	Ce, La
42	Sitges	HS concentrated	Isolated	Aggregate	1653	Elongated	Ce, La
43	Sitges	HS concentrated	Isolated	Aggregate	1016	Roundish	Ce, La
44	Sitges	Control sample	Isolated	Aggregate	2067	Roundish	Ce, La, Nd

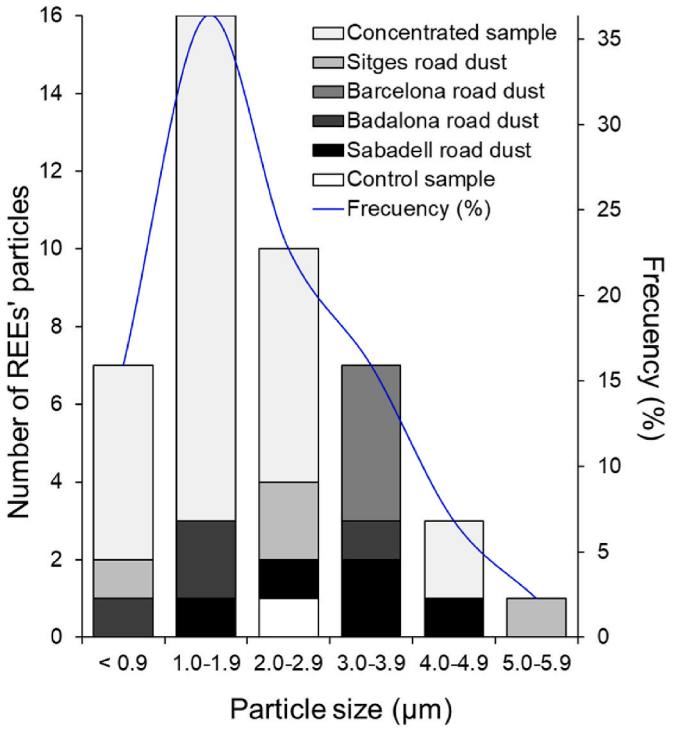

Fig. 4. Histogram of REEs' particle size distribution curve determined from the FE-SEM images.

some of the heavy particles incrusted on the monolayers (Fig. 5b), which indicates that they were not completely polished. All of these facts exclude the possibility of sample contamination by the polishing material used.

Although the identified REEs' grains morphology is quite diverse, their habits were classified as equant and inequant. In addition, well-developed crystalline facets or euhedral crystal shapes were not observed. Some particles (23%) exhibited equant habits with perfectly spheric shapes and no surficial irregularities, but two of them display rugged surface with a few adhered nanoparticles (<50 nm) (Fig. 5c). Most REEs' grains (77%) showed inequant habits with rounded (Fig. 5a, **d** and **e**), elongated (Fig. 5f, **g**, **h** and **i**), as well as edgy shapes (Fig. 5b, **j**, **k** and **l**). 24 of the investigated REE's particles were monocrystalline, whereas the other 20 consisted of aggregates of nanoparticles whose sizes are less than 100 nm across (Table 2 and Fig. 5). Spheric and edgy particles were mostly monocrystalline (100 and 82%, respectively), whereas those with rounded and elongated shapes were mainly constituted by aggregates of nanoparticles (75 and 83%, respectively). These aggregates exhibited framboidal and botryoidal morphologies due to the nanoparticle spheroidal shapes (Fig. 5d and **g**). They also showed rosette-like habits with a surficial spongy texture due to nanoplate superposition (Fig. 5h and **i**). In addition, the size of nanoplates (Fig. 5i) was commonly larger than the nanospheres (Fig. 5d). Furthermore, carbonate and iron nanoparticles with worm-like textures were observed adhered to the surface of REEs' grains (Fig. 5c, **e** and **j**).

The REEs' particles identified in the present study were compositionally characterized by containing only light REEs (LREEs: La to Eu). Due to the small particle size (avg. 2.1 μm) and the EDS spot size (~2 μm), an accurate mineral phase determination was not possible. Nevertheless, it was confirmed that REEs' grains always contained Ce and different La and Nd proportions, depending on the particle morphology (Table 2 and Fig. 5): i) spheric REEs' particles (23% of the particles) contained Ce and, a few smallest particles, also La; ii) rounded particles, the most abundant morphology (27%), commonly had La in trace amounts and, more rarely, Nd; iii) elongated particles (25%) have significant proportions of La, Nd, or La–Nd; and iv) edgy particles (25%) are mainly composed of both Ce and La.

The lack of phosphorous, silica and carbon peaks in the EDS analyses suggests that the road dust REEs' particles from Barcelona might correspond to cerium oxide. It should be noted that no U nor Th content was detected under EDS. All this agrees with the recent XRD identified ceria (CeO_2) particles, on road dust samples from Hermosillo city (Mexico), which have crystal sizes of 10–30 nm (Meza-Figueroa et al., 2021).

3.1.2. Other heavy metal particles

Barium sulfate ($BaSO_4$) crystals were found in all the studied localities (>150 analyzed particles). These particles exhibited euhedral to subhedral morphologies and sizes of less than 10 μm and occurred as isolated crystals or as particles adhered to larger ones, constituted by Ca–Fe silicates (Fig. 6a) and native Fe and Fe-alloys (Fig. 6b). Pb, Sn, Cu and Sb sulfides of less than 100 μm long (>50 grains; Fig. 6c, **d** and **e**) were also identified. In addition, other minor sulfides constituted by Fe–Cu, Zn and Fe were found but not shown in Fig. 6, which may correspond to galena, stannite, covellite, chalcopyrite, sphalerite, pyrite, and stibnite crystals, respectively. Native Fe particles, in some cases Fe-oxides, were abundant and presented diameters that ranged from 50 to 100 μm (58 investigated particles; Fig. 6f), although some particles were smaller than 10 μm in size. Moreover, abundant native Pb particles, and to a lesser extent native Cu, W and Sn grains (41 particles: Fig. 6g, **h**, **i** and **j**), as well as Fe–Ti (Fig. 6b), Fe–Cr (Fig. 6k), Fe–Ni (Fig. 6l), Cu–Zn (Fig. 6e), and Bi–Fe (Fig. 6m) alloys were identified. Exceptionally, particles with unusual composition were observed: Au–Pd alloys of <10 μm (Fig. 6n), an exotic indium oxide aggregate of 20 μm (probably In_2O_3) covered by native Sn and Bi–Pb alloy crystals (Fig. 6j), and zirconium oxide (probably zirconia: ZrO_2) rounded microparticles (2 particles: Fig. 6o).

3.2. Geochemical and mineralogical tools for roadside dust source identification

3.2.1. Global values of metal enrichment factors

The Enrichment Factor (EF_x) was defined to evaluate the magnitude of chemical contaminants in street and road dust and to differentiate anthropogenic from geogenic metal sources (e.g., Reimann and Caritat, 2000):

$$EF_x = (X_i/E_{ref})_{sample}/(X_i/E_{ref})_{background}$$

where x is the element of interest, X_i is the concentration of the element and E_{ref} the reference element concentration for normalization. Commonly, the average upper continental crust (UCC) reference values (Rudnick and Gao, 2003) are used as background levels. The element of reference E_{ref} should be characterized by a low variability occurrence. Nevertheless, there is no consensus on its choice; some authors use Ti (Morera-Gómez et al., 2020), others Mn (Yongming et al., 2006; Dytlow and Górka-Kostrubiec, 2021), Al (Taghavi et al., 2017; Ulutaş, 2022), Sc (Najmeddin et al., 2018; Abbasi et al., 2018) or even a combination of different elements (Ca, Mg, Al, Na, K, P and Ti: Varrica et al., 2003; Sc, Fe, Al, Ti, and Mn: Akbari et al., 2022; Al, Fe, Ti, Si, Sr and K: Han et al., 2018). A literature compilation of EF_x data from analyzed dust for several heavy metals is plotted in Fig. 7.

Routinely, an element is considered to have a geogenic origin when its EF_x is close to 1, whereas the element is supposed to have an anthropogenic source when the $EF_x > 10$, regardless of the chosen reference E_{ref} (e.g., Nolting et al., 1999). For instance, Zn, Pb, Sb, Cr, Ni, Cu, Mo, Fe, Sn, Ba and Cr on worldwide road dust have EF_x values that commonly range from >2 to more than 100 (Fig. 7). The observed extremely high EF_x values for these elements suggest they might have an anthropogenic origin. Indeed, these high values are also consistent with the abundance of Fe, Cu, Zn, Ni, Cr and Pb sulfates, sulfides, native

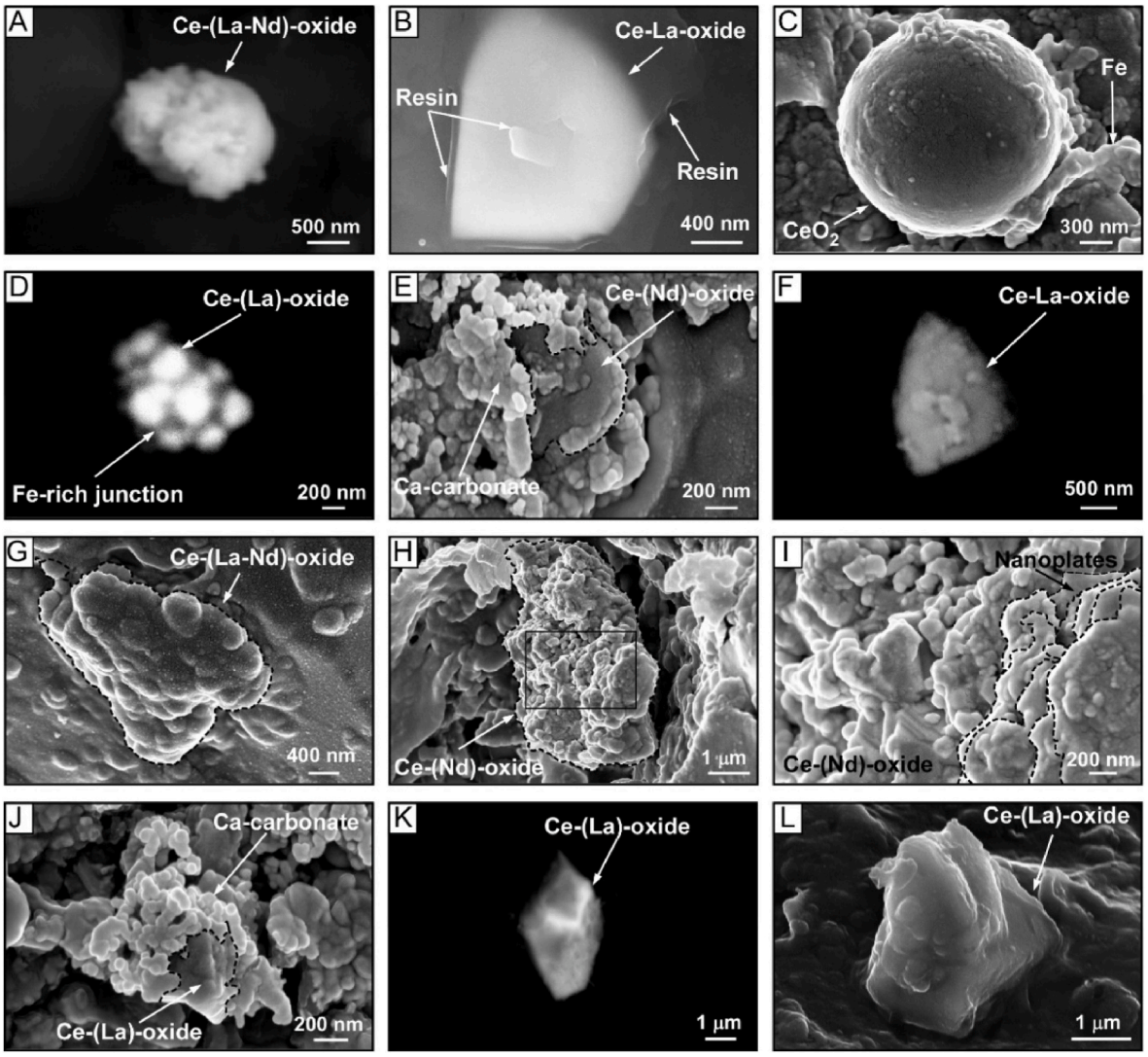

Fig. 5. Morphological and textural details of REEs' particles of the investigated roadside dust samples. A, D, F and K are backscattered electron images whereas B, C, E, G, H, I, J and K are secondary electron images obtained by means of FE-SEM. **A)** Particle aggregate with rounded morphology and spongy texture of Ce-(La–Nd)-oxide nanoparticles. **B)** Ce-(La)-oxide edgy particle covered by a thin film of resin of the monolayer preparation. **C)** Spheric grain with some adhered nanoparticles and native Fe film. **D)** Framboidal nanoparticle aggregate of Ce-(La)-oxide. **E)** Rounded Ce-(Nd)-oxide particle covered by Ca carbonate nanoparticles. **F)** Ce-(La)-oxide with elongated shape. **G)** Botryoidal Ce-(La–Nd)-oxide elongated grain constituted by nanoparticles aggregates. **H)** Elongated aggregate of Ce-(Nd)-oxide nanoparticles with platy shapes. **I)** Details from (H), showing superposed nanoplates of REEs with rosette-like and spongy textures. **J)** Ce-(La)-oxide particle covered by Ca carbonate nanoparticles. **K)** Edgy Ce-(La)-oxide particle. **L)** Edgy Ce-(La)-oxide particle aggregate. Dashed lines correspond to investigated ceria particles.

elements, and alloys observed in the studied road dust from the Barcelona area (Fig. 6).

Although the use of EF_x values can be appropriate tracers for some common road dust' elements (e.g., Ba, Pb, Sb, Sn, Fe, Zn, Cu, Sn, Ni, Mo and Cr; Fig. 7), there are some shortcomings that must be considered (Reimann and Caritat, 2000): i) the type of reference substrate, as there is a large variability in trace element contents even among rocks with similar bulk composition; ii) the element fractionation during their transfer from crust to atmosphere, and iii) the biogeochemical impact processes, that might change the original concentrations of these elements. Moreover, some elements with an anthropogenic origin accumulate in road dust at concentrations within the range of the geogenic substrate background (e.g., UCC, local substrate baseline). Consequently, the EF_x for these elements would show values around 1 and hence they might be mistakenly attributed to have a geogenic origin. This is commonly the case for REEs (Fig. 8). Therefore, the use of EF_x values for emergent particulate pollutants that appear in low concentration in road dust might not be an appropriate tool to identify their potential sources.

3.2.2. *Ternary plots: worldwide geochemical data*

Ternary plots of La and Ce contents combined with other trace elements (e.g., La–Ce-Sm, La–Ce–V, La–Ce–As) are extensively used as chemical tracers of oil refineries, exhaust traffic, coal and oil combustions, as well as ceramic industry emissions (e.g., Moreno et al., 2008a, b; Moreno et al., 2010; Moreno et al., 2013). For instance, Moreno et al. (2008a, b), introduced the ternary La–Ce–V diagram (Fig. 9) to discriminate anthropogenic from geogenic source for REEs in airborne PM of 2.5 µm ($PM_{2.5}$) and 10 µm (PM_{10}). According to this diagram, the La–Ce–V global $PM_{2.5}$ and PM_{10} compositions plot in two groups (Fig. 9): i) a group with most values aligned between a hydrocarbon combustion source and the emissions from combustion vehicles using autocatalytic converters, crossing the UCC composition; and ii) a small number of values that plot aligned between a hydrocarbon combustion

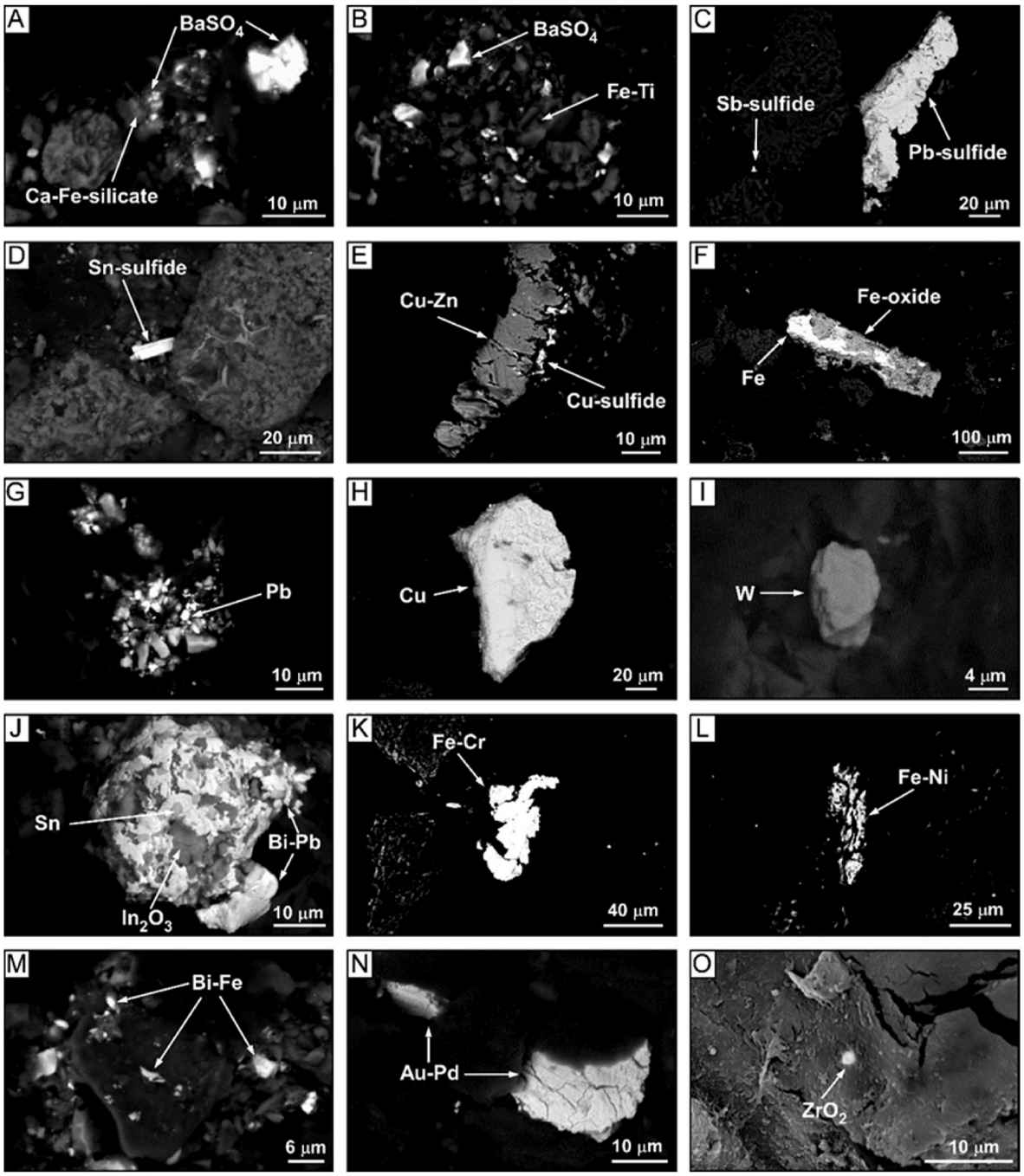

Fig. 6. Backscattered electron images showing textural details of sulfates, sulfides, oxides, native elements and metal alloy particles in the roadside dust of Barcelona obtained by means of SEM. **A)** Barium sulfate ($BaSO_4$) as an isolated particle and adhered grains into native Fe particles. **B)** $BaSO_4$ clusters adhered to Ca–Fe silicates. **C)** Isolated Pb sulfide microparticle and Sb sulfide grain adhered onto a silicate particle. **D)** Isolated Sn sulfide. **E)** Cu sulfide grains associated with a Cu–Zn alloy. **F)** Native Fe highly altered to Fe-oxide. **G)** Native Pb clusters. **H)** Microparticle of native Cu. **I)** Native W grain. **J)** Indium oxide particle coated by Bi–Pb alloys and native Sn grains. **K)** Isolated Fe–Cr alloy microparticle. **L)** Fe–Ni alloy grain. **M)** Bi–Fe alloy clusters. **N)** Exotic Au–Pd alloys. **O)** Adhered zirconia (ZrO_2).

source and emissions from oil refineries using Fluid Catalytic Cracking (FCC). As the data plot in the ternary diagram between the combustion vehicles using TWCCs and the uncontaminated crustal material composition, the involvement of both sources is suggested. Nevertheless, the data can also reflect a major proportion of particles sourced from TWCCs rather than from oil combustion (Fig. 9). Consequently, La–Ce–V tracer tool is not capable of discriminating geogenic from anthropogenic sources when a sample plots between the TWCCs and oil end-members, which is the most typical range of global $PM_{2.5}$, PM_{10} and road dust (Fig. 9).

3.2.3. *A mineralogical tool to identify the source of heavy metal particles*

Most of the identified sulfates, sulfides, oxides, and alloys (Figs. 5 and 6) from the studied roadside dust samples are commonly small constituents of transport vehicles. REEs' road dust particles show identical morphologies, grain size ranges, chemical characteristics, and occurrences, in all the investigated localities of the Barcelona area (Table 2 and Fig. 5): spherical, rounded, elongated or edgy shapes of Ce-oxide composition, usually enriched with La with Nd, which occur as discrete or adhered single crystals and aggregates of nanoparticles. The large number of REEs' particles and aggregates found in the

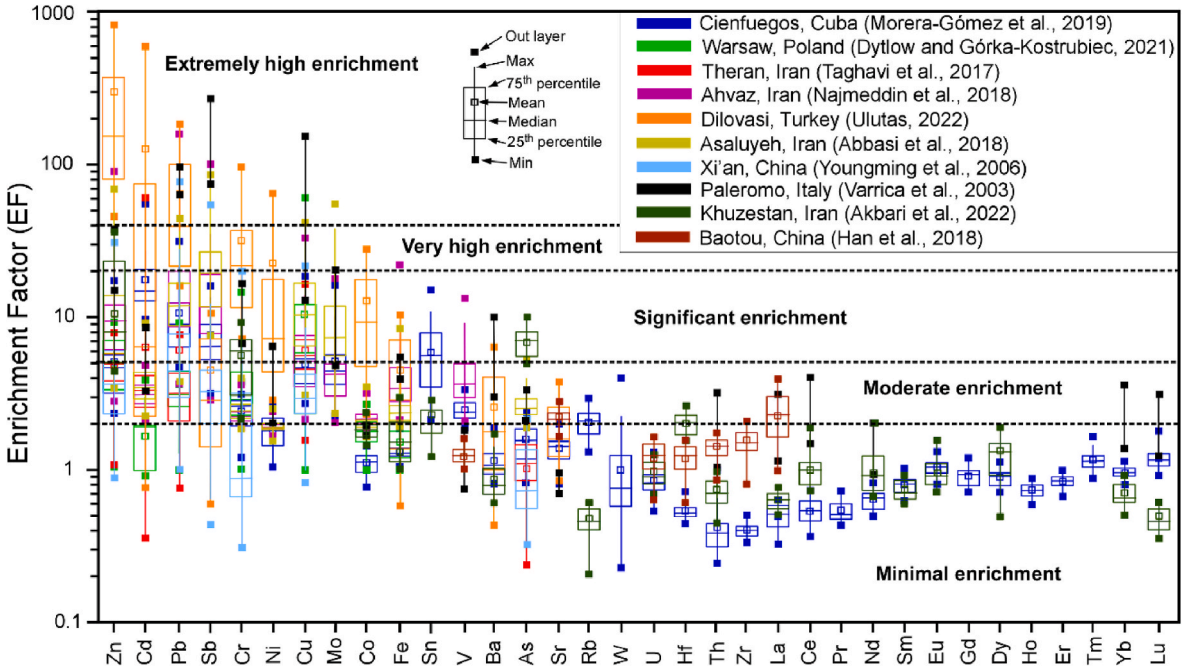

Fig. 7. Box-plot of EF_x values for trace elements in road dust of some cities around the globe.

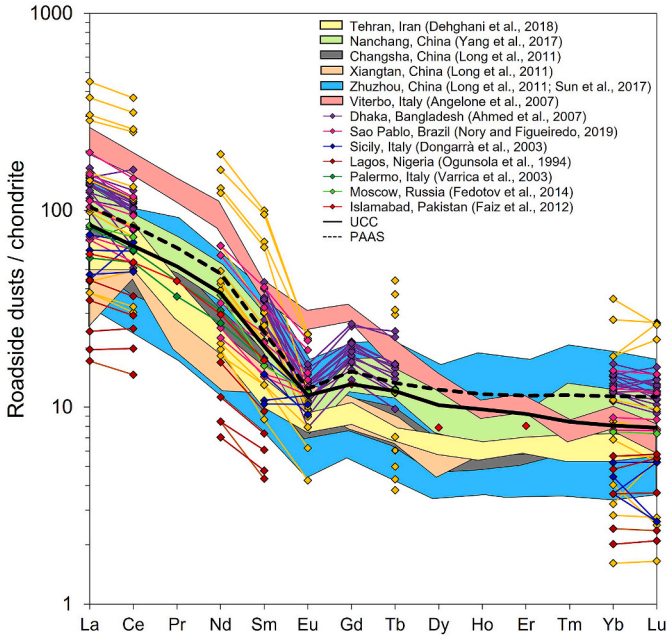

Fig. 8. Chondrite-normalized REEs distributions of worldwide roadside dust. Chondrite normalization values after McDonough and Sun (1995). Note that global roadside dust show the same REEs' pattern and similar concentrations than the average Upper Continental Crust (UCC: Rudnick and Gao, 2003) and Post Archean Australian Shales (PAAS: Taylor and McLennan, 1995) reference values.

concentrated samples (Table 2 and Fig. 5) prove that the hydro-separation technique is very effective in concentrating REEs' particles in urban dust.

Due to the fact that the sample areas are located at different geologic backgrounds with dissimilar lithologies (Fig. 1), the shared chemical and morphological characteristics of the CeO_2 particles from all sampling sites are independent of the geologic substrate. Indeed, these particles must have originated from a common anthropogenic source. Additionally, the mineralogical features of most heavy particles from the studied road dust (sulfates, sulfides, oxides and alloys; Fig. 6) also point to an anthropogenic origin. For instance, it is known that barium sulfate is used as brake pad composites, similarly to metal sulfides as covellite, sphalerite, pyrite, chalcopyrite, and stibnite, as well as metallic Cu (e.g., Amato et al., 2011). Consequently, the presence of these mineral phases in the studied road dust are probably related to the degradation of vehicles' brake linings and, thus, they may have an anthropogenic origin. On the other hand, native Pb and Sb particles can be sourced to gasoline combustion (Ondov et al., 1982; Pacyna et al., 1984). Additionally, metallic Fe and alloys of different composition, as Fe–Ni and Fe–Cr, are typically applied as electrodeposition film on stainless steel (e.g., Bertero et al., 2018).

The synthetic CeO_2 used on TWCCs has a fluorite type structure for their thermal stability (Trovarelli, 1996) and is commonly dopped with high amounts of La (e.g., $Ce_{0.8}La_{0.2}O_{2-x}$) and Nd, among other LREEs, to enhance their oxygen storage capacity (e.g., Higashi et al., 1999; Anjaneya et al., 2016). In contrast, geogenic CeO_2, the mineral cerianite, which is one of the scarcest REEs' minerals in natural environments, contains significant U and Th as trace elements, and typically lower LREE contents than the synthetic LREE-doped version, ceria (Graham, 1955; Zaitsev et al., 2011). Since its discovery in the 1950s, no more than 100 reliable world finds of the natural CeO_2 mineral, mainly in the form of discrete euhedral microcrystals (~5 μm) with intergrowths and microinclusions in other minerals, have been documented (e.g., Graham, 1955; Skublov et al., 2009; Zaitsev et al., 2011). The absence of euhedral crystals, microinclusions and of U and Th traces in all the studied road dust Ce-oxide particles, as well as the high La content, agrees with an origin related to the TWCC washcoats.

3.3. Formation mechanism of REEs' particles

It has been widely documented that the TWCCs abrasion and wear result in the emission of ZrO_2–CeO_2 particles, ceria, and zirconia, into the environment (Meza-Figueroa et al., 2021; Navarro-Espinoza et al., 2022). Therefore, the presence of spheroidal microparticles of zirconia in the investigated road dust (Fig. 6o) is also consistent with an anthropogenic source. Navarro-Espinoza et al. (2022) suggested that ZrO_2 is released to the environment from an initial $Ce_xZr_{1-X}O_2$ solid

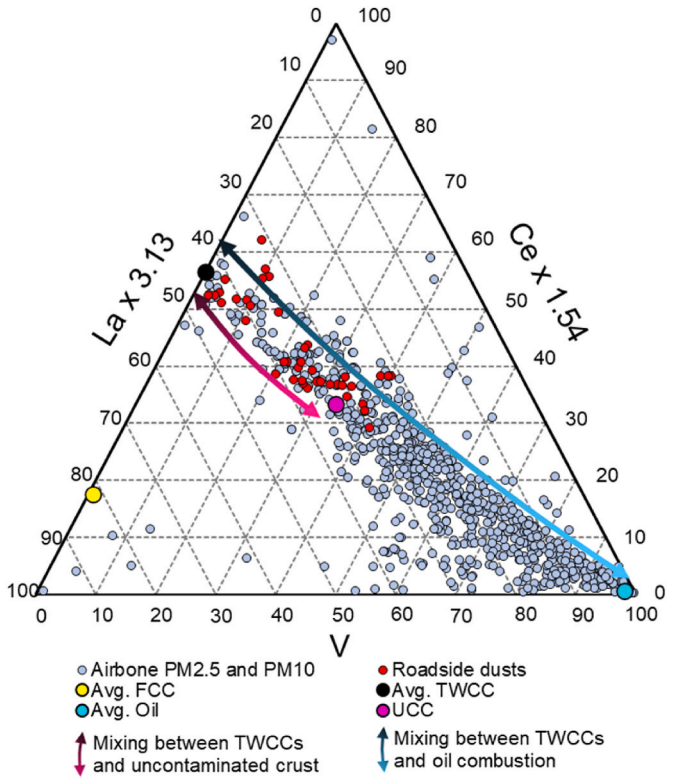

Fig. 9. La–V–Ce ternary plot for the worldwide road dust (red dots) and airborne $PM_{2.5}$ and PM_{10} (blue dots) from literature data (Olmez and Gordon, 1985; Ogunsola et al., 1994; Wang et al., 2000; Dongarrà et al., 2003; Varrica et al., 2003; Kulkarni et al., 2007; Moreno et al., 2006, 2008a, 2008b, 2013; Castillo et al., 2006; Amato et al., 2011; Sánchez et al., 2011; Celo et al., 2012; Faiz et al., 2012; Valdés et al., 2013; Conca et al., 2019; Bozlaker et al., 2019; Adon et al., 2020). Average chemical composition of emissions from oil refineries using zeolitic fluid catalytic converters (FCC: Olmez et al., 1988; Kitto et al., 1992; Kulkarni et al., 2006; Ferella et al., 2019), combustion vehicles using autocatalytic converters (TWCCs: Chellam and Bozlaker, 2015), hydrocarbon combustion (fuel oils and petcoke: Olmez et al., 1988; Duyck et al., 2008; Zhang et al., 2009; Yasnygina et al., 2015), and Upper Continental Crust (UCC: Rudnick and Gao, 2003) are represented.

solution, whereas CeO_2 remains in the Al_2O_3 layer of TWCCs, forming a $Al_xCe_{1-X}O_2$ composite. Nevertheless, our study reveals that the CeO_2 particles can also be released to the environment. Ceria particles and nanoparticles described in the present study are not enriched in Zr nor Al, and zirconia does not contain Ce traces, which suggests that they are not directly related to the mechanical extraction from the TWCCs' washcoat. Instead, it is proposed that zirconia and ceria particles must have been released to the environment as separate phases. This opens the door to the possibility that these particles could be neo-formed phases.

Numerical simulations suggest that $Ce_xZr_{1-X}O_2$ is metastable and separates into zirconia and ceria particles at the operation temperatures of TWCCs in modern cars, which can reach ~1100 °C (Grau-Crespo et al., 2011). At these high temperatures, crystal growth and recrystallization of phases by sintering is possible, causing a reduction in the specific surface area of the new nanostructured CeO_2 and, in consequence, an increase of particle size and multifaced morphologies (Fig. 10), thus generating less reactive edge sites (Reddy and Khan, 2005). On the other hand, Navarro-Espinoza et al. (2022) identified spheroidal particles with smaller diameters (50–200 nm) in non-degraded TWCCs than in degraded ones (diameters of 100–400 nm). Experimental studies (e.g., Zaengle et al., 2020) have also shown that ceria particles at low sintering temperatures are characterized by spheroidal morphologies and reduced sizes, whereas at higher temperatures they display multifaceted shapes and sizes. These results can explain the fact that the average size of the studied monocrystalline spheroidal and rounded ceria particles was lower (1.9 ± 1.6 μm; n = 13) than the elongated and edgy particles (2.3 ± 1.1 μm; n = 11). Consequently, the precursor spheroidal ceria particles on washcoat TWCCs could have recrystallized to multifaced shapes at higher temperature conditions (Fig. 10).

During sintering of TWCCs' particles, a migration of the more mobile atoms occurs at the crystal surface, driven by differences in free energy and local concentrations of atoms (adatom, Ostwald Ripening sintering mechanism: OR; Hansen et al., 2013). This can explain the common absence of La and Nd in road dust' ceria spheroidal particles and the enrichment of these elements in rounded, elongated, and edgy grains (Table 2). La and Nd could have migrated from spheroidal particles to more surficial parts, incorporating recrystallized ceria particles in higher proportions by sintering (Fig. 10). Furthermore, this process agrees with the varied La and Nd contents in the rounded, elongated and edgy ceria particles found in this study (Table 2).

Moreover, sintering in the TWCCs causes the mobility of particles on the monolith surface followed by a coalescence that leads to the growth of the particles (Particle Migration-Coalescence mechanism process: PMC; Hansen et al., 2013). Fig. 5a shows a rounded ceria particle with local nanoaggregate adhesions at its surface, which could reflect this particle coalescence process. The bigger size of the identified ceria monocrystalline particles (avg. 2.1 μm; Table 2 and Fig. 5) relative to the precursor spheroidal nanoparticles (<100 nm; Navarro-Espinoza et al., 2022), which are commonly observed as a nanoaggregate microparticles (Fig. 5e), is also consistent with the sintering PMC mechanism. In addition, the crystalline growth by sintering is consistent with the morphological differences of the ceria nanoparticles: the precursor nanospheres could have recrystallized to more multifaced shapes generating larger nanoplates (Fig. 5h). Then, the larger sintered particles would have reduced their adhesion to the substrate, making them more easily detachable from the washcoat TWCCs and hence more easily released to the environment (Fig. 10).

3.4. Further considerations

A detailed mineralogical study of road dust' particles may substantially improve the geochemical limitations to identify their potential sources as in the present study. In addition, the characterization of road dust REEs' particles by means of visual observations and in situ chemical analyses will be advantageous for future ecologic and human health studies. Microparticles of less than 5 μm, and more commonly around 1 μm, can be easily inhaled; therefore, REEs' particles with sizes smaller than 2.5 μm can reach the deepest part of the lungs and cause granulomatous lesions and pneumoconiosis (Sabbioni et al., 1982; Pagano et al., 2015). The morphology, size and mineral chemical composition of the REEs' particles may play a key on environmental processes, such as: i) particle resuspension into the atmosphere (e.g., Tian et al., 2019) and transference to adjacent soils (Figueiredo et al., 2009); ii) dissolution rate of REE oxides in urban runoff stormwater (Shajib et al., 2020) and transport along natural waters; and iii) phytoaccumulation of REEs onto above-ground plant organs (Djingova et al., 2003; Mikołajczak et al., 2017; Mleczek et al., 2018). These processes could facilitate road dust' ceria particles entering the human body not merely via inhalation, but also through direct ingestion, that is with drinking water and food. For these reasons, the ceria particles emitted by vehicles are a significant environmental health hazard, which reveals the need for further investigation and levels assessment of the emerging particle pollutant ceria generated by automobiles in urban areas worldwide.

4. Conclusions

This study provides new insights into the source, release, and

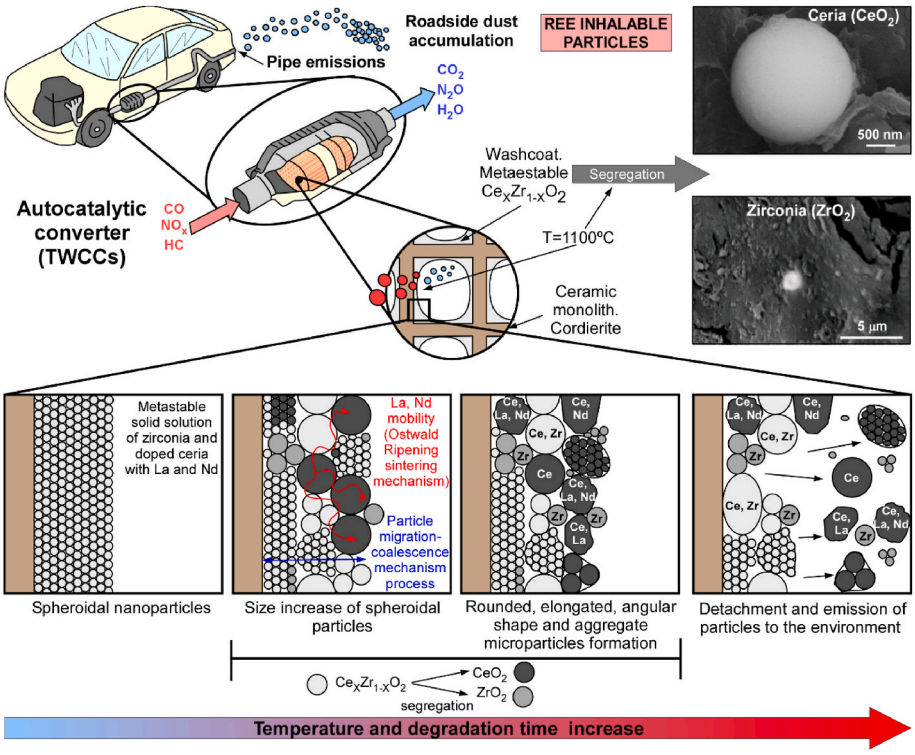

Fig. 10. Proposed genetic model for road dust ceria particle formation.

environmental accumulation processes of REEs' particles and nanoparticles from road dust by means of direct mineralogical visual investigations and chemical analysis. Inhalable particles and nanoparticles of CeO_2 were identified in road dust using a combination of hydroseparation technique (HS-11), to concentrate fine dense particles, and electronic microscopes (SEM-EDS and FE-SEM-EDS) for their visual identification and characterization. This reveals the potential of the combined techniques for the study of dense particles of small size (<30 μm) which are present in very low concentrations in the bulk sample. In this study, it is also shown that bulk chemical studies alone cannot account for a reliable tool to identify the source of the REEs' particles; however, a detailed mineralogical study of the ceria particles has proved to be a good alternative to identify their potential source.

The observed REEs' particles from the studied road dust samples show identical morphologies, grain size ranges, chemical characteristics, and occurrences in all the investigated localities; they are spheroidal, rounded, elongated or edgy Ce-oxide micro and nanoparticles, usually enriched with La and in lesser extend with Nd, which occur as discrete or adhered single crystals and nanoaggregates. These common characteristics, independently of the lithologies present in their geological location, point to an anthropogenic source related to vehicle emissions. The CeO_2 (ceria) particles might form by separation from the $CeZrO_x$ metastable phase at the washcoat vehicles' autocatalyzer. The ceria particles of the investigated roadside dust could be formed during a sintering at the operation temperatures of the autocatalyzer, which would produce a reduction in the specific surface area of nanostructured ceria, as well as an increase of particle size and multifaceted shapes. These results also show that urban traffic is an important source of inhalable ceria particles which might pose an environmental health hazard. Nevertheless, further studies are needed to better assess this pollutant.

Funding

This research was funded by POC2022_2 to D. Navarro and M. Corbella granted by the Universitat Autònoma de Barcelona (Proof of Concept), the Spanish projects PID2019-109018RB-I00 to M. Corbella granted by the Spanish Ministerio de Ciencia e Innovación (MICINN) and Caribbean Lithosphere Research Group (http://caribbeanlithos.ub.edu). Support for the research was received also through the project 2022-SGR-00308 (Consolidate Research Group MAG) from the Catalan Government of Spain.

CRediT authorship contribution statement

Dídac Navarro-Ciurana: Project administration, Supervision, Conceptualization, Methodology, Resources, Funding acquisition, Formal analysis, Investigation, Visualization, Writing – original draft, Writing – review & editing. **Mercè Corbella:** Resources, Funding acquisition, Investigation, Writing – review & editing, Supervision. **Júlia Farré-de-Pablo:** Methodology, Writing – review & editing. **Isaac Corral:** Methodology, Writing – review & editing. **Elisabeth Buixadera:** Resources, Methodology. **Robert Morera-Valverde:** Resources, Methodology. **Joaquín A. Proenza:** Resources, Investigation, Writing – review & editing.

Declaration of competing interest

The authors declare the following financial interests/personal relationships which may be considered as potential competing interests: Didac Navarro reports financial support was provided by Universitat Autònoma de Barcelona (Proof of Concept). Merce Corbella reports was provided by Spanish Ministerio de Ciencia e Innovación.

Data availability

None.

Acknowledgements

The authors would like to acknowledge the technicians of the Servei de Microscòpia of Universitat Autònoma de Barcelona for their support

in SEM-EDS and FE-SEM-EDS investigations. We would like to thank anonymous referees for their critical and valuable reviews, as well as Associated Editor Song Guo for handling this manuscript.

References

Abbasi, S., Keshavarzi, B., Moore, F., Mahmoudi, M.R., 2018. Fractionation, source identification and risk assessment of potentially toxic elements in street dust of the most important center for petrochemical products, Asaluyeh County, Iran. Environ. Earth Sci. 77, 673. https://doi.org/10.1007/s12665-018-7854-z.

Adon, A.J., Liousse, C., Doumbia, E.T., Baeza-Squiban, A., Cachier, H., Léon, J.F., Yoboue, V., Akpo, A.B., Galy-Lacaux, C., Zoutien, C., Xu, H., Gardrat, E., Keita, S., 2020. Physico-chemical characterization of urban aerosols from specific combustion sources in West Africa at Abidjan in Côte d'Ivoire and Cotonou in Benin in the frame of DACCIWA program. Atmos. Chem. Phys. 20, 5327–5354. https://doi.org/10.5194/acp-20-5327-2020.

Aiglsperger, T., Proenza, J.A., Zaccarini, F., Lewis, J.F., Garuti, G., Labrador, M., Longo, F., 2015. Platinum group minerals (PGM) in the falcondo Ni-laterite deposit, loma caribe peridotite (Dominican republic). Miner. Depos. 50, 105–123. https://doi.org/10.1007/s00126-014-0520-9.

Akbari, Z., Kakuee, O., Shahbazi, R., Khatooni, J.D., Mashal, M., 2022. Application of positive matrix factorization and pollutants tracing for identification of dust sources: a case study in Khuzestan, Iran. Environ. Eng. Res. 27, 210365 https://doi.org/10.4491/eer.2021.365.

Amato, F., Pandolfi, M., Moreno, N., Furger, M., Pey, J., Alastuey, A., Bukowiecki, N., Prevot, A.S.H., Baltensperger, U., Querol, X., 2011. Sources and variability of inhalable road dust particles in three European cities. Atmos. Environ. 45, 6777–6787. https://doi.org/10.1016/j.atmosenv.2011.06.003.

Anadón, P., Cabrera, L., Guimerà, J., Santanach, P., 1985. Paleogene strike-slip deformation and sedimentation along the southeastern margin of the Ebro Basin. In: Biddle, K.T., Christie-Blick, N. (Eds.), Strike-Slip Deformation, Basin Formation, and Sedimentation. SEPM Society for Sedimentary Geology: Broken Arrow, OK, USA, pp. 303–318.

Anadón, P., Colombo, F., Esteban, M., Marzo, M., Ribles, S., Santanach, P., Solé Sugrañés, Ll, 1979. Evolución tectonoestratigráfica de los Catalánides. Acta Geol. Hisp. 43, 242–270.

Anjaneya, K., Manjanna, J., Ashwin Kumar, V., Jayanna, H., Naveen, C., 2016. Rare Earth ion doped ceria as electrolytes for solid oxide fuel cell. Adv. Mater. Lett. 7, 743–747. https://doi.org/10.5185/amlett.2016.6070.

Bertero, E., Hasegawa, M., Staubli, S., Pellicer, E., Herrmann, I.K., Sort, J., Michler, J., Philippe, L., 2018. Electrodeposition of amorphous Fe-Cr-Ni stainless steel alloy with high corrosion resistance, low cytotoxicity and soft magnetic properties. Surf. Coat. Technol. 349, 745–751. https://doi.org/10.1016/j.surfcoat.2018.06.003.

Bozlaker, A., Chellam, S., 2015. Measurement of the trace element composition of airborne particulate matter and its use in source apportionment: case studies of lanthanoids and platinum group metals from Houston, TX. In: Evans, K., Lanigan, K., Roberts-Kirchhoff, R., Rihana, A., Benvenuto, M. (Eds.), Trace Materials in Air, Soil, and Water, vol. 1210. American Chemical society, pp. 3–36 (Chapter 1).

Bozlaker, A., Prospero, J., Price, J., Chellam, S., 2019. Identifying and quantifying the impacts of advected North African dust on the concentration and composition of airborne fine particulate matter in Houston and Galveston, Texas. J. Geophys. Res. Atmos. 124, 12282–12300. https://doi.org/10.1029/2019JD030792.

Cabri, L.J., Rudashevsky, N.S., Rudashevsky, V.N., Gorkovetz, V.Y., 2008. Study of native gold from the Luopensulo deposit (Kostomuksha area, Karelia, Russia) using a combination of electric pulse disaggregation (EPD) and hydroseparation (HS). Miner. Eng. 21, 463–470. https://doi.org/10.1016/j.mineng.2008.02.006.

Castillo, S., Moreno, T., Querol, X., Alastuey, A., Cuevas, E., Herrmann, L., Mounkaila, M., Gibbons, W., 2006. Trace element variation in size-fractionated African desert dusts. J. Arid Environ. 72, 1034–1045. https://doi.org/10.1016/j.jaridenv.2007.12.007.

Celo, V., Dabek-Zlotorynska, E., Zhao, J., Bowman, D., 2012. Concentration and source origin of lanthanoids in the Canadian atmospheric particulate matter: a case study. Atmos. Pollut. Res. 3, 270–278. https://doi.org/10.5094/APR.2012.030.

Chakhmouradian, A.R., Wall, F., 2012. Rare earth elements: minerals, mines, magnets (and more). Elements 8, 333–340. https://doi.org/10.2113/gselements.8.5.333.

Chellam, S., Bozlaker, A., 2015. Characterization of PGEs and other elements in road dusts and airborne particles in Houston, Texas. In: Zereini, F., Wiseman, C. (Eds.), Platinum Metals in the Environment. Environmental Science and Engineering. Springer, Heidelberg, Berlin, pp. 199–242. https://doi.org/10.1007/978-3-662-44559-4_14.

Clement, N., Muresan, B., Hedde, M., Francois, D., 2015. Assessment of palladium footprint from road traffic in two highway environments. Environ. Sci. Pollut. Res. 22, 20019–20031. https://doi.org/10.1007/s11356-015-5241-9.

Conca, E., Abollino, O., Buoso, S., Traversi, R., Becagli, S., Grotti, M., Malandrino, M., 2019. Source identification and temporal evolution of trace elements in PM_{10} collected near to Ny-Ålesund (Norwegian Arctic). Atmos. Environ. 203, 153–165. https://doi.org/10.1016/j.atmosenv.2019.02.001.

Dehghani, S., Moorea, F., Vasiluk, L., Haleb, B.A., 2018. The geochemical fingerprinting of geogenic particles in road deposited dust from Tehran metropolis, Iran: implications for provenance tracking. J. Geochem. Explor. 190, 411–423. https://doi.org/10.1016/j.gexplo.2018.04.011.

Dey, S., Mehta, N.S., 2020. Automobile pollution control using catalysis. Res. Environ. Sustain. 2, 100006 https://doi.org/10.1016/j.resenv.2020.100006.

Djingova, R., Kovacheva, P., Wagner, G., Markert, B., 2003. Distribution of platinum group elements and other traffic related elements among different plants along some highways in Germany. Sci. Total Environ. 308, 235–246. https://doi.org/10.1016/S0048-9697(02)00677-0.

Dongarrà, G., Sabatino, G., Triscari, M., Varrica, D., 2003. The effects of anthropogenic particulate emissions on roadway dust and Nerium oleander leaves in Messina (Sicily, Italy). J. Environ. Monit. 5, 766–773. https://doi.org/10.1039/B304461K.

Duyck, C., Miekeley, N., Fonesca, T., Szatmari, P., Vaz dos Santos Neto, E., 2008. Trace element distributions in biodegraded crude oils and fractions from the Potiguar Basin, Brazil. J. Braz. Chem. Soc. 19, 978–986. https://doi.org/10.1590/S0103-50532008000500025.

Dytłow, S., Górka-Kostrubiec, B., 2021. Concentration of heavy metals in street dust: an implication of using different geochemical background data in estimating the level of heavy metal pollution. Environ. Geochem. Health 43, 521–535. https://doi.org/10.1007/s10653-020-00726-9.

EEA, 2019. Quality in Europe, 2019 Report. Publications Office of the European Union, Luxembourg, p. 104, 2019.

Faiz, Y., Siddique, N., Tufail, M., 2012. Pollution level and health risk assessment of road dust from an expressway. J. Environ. Sci. Heal. A. 47, 818–829. https://doi.org/10.1080/10934529.2012.664994.

Ferella, F., Adamo, I., Leone, S., Innocenzi, V., Michelis, I., Vegliò, F., 2019. Spent FCC E-Cat: towards a circular approach in the oil refining industry. Sustainability 11, 113. https://doi.org/10.3390/su11010113.

Figueiredo, A.M.G., Camargo, S.P., Sígolo, J.B., 2009. Determination of REE in urban park soils from São Paulo city for fingerprint of traffic emission contamination. In: International Nuclear Atlantic Conference – INAC 2009, Rio de Janeiro, pp. 1–7.

Gómez, M., Guimerà, J., 1999. Estructura alpina de la serra de Miramar y del NE de las muntanyes de prades (Cadena costero catalana). Rev. Soc. Geol. España, pp. 405–418.

Graham, A.R., 1955. Cerianite CeO_2: a new rare-earth oxide mineral. Am. Mineral. 40, 560–564.

Grau-Crespo, R., De Leew, N., Hamad, S., Umesh, W., 2011. Phase separation and Surface segregation in ceria-zirconia solid solutions. Proc. R. Soc. A A. 467, 1925–1938. https://doi.org/10.1098/rspa.2010.0512.

Guimerà, J., 1983. Palaeogene evolution of deformation in the northeastern Iberian Peninsula. Geol. Mag. 121, 413.

Guimerà, J., De Vicente, G., Rodríguez Pascua, M.A., Muñoz Martín, A., Vegas, R., Simón, J.L., 2004. Cadenas con cobertura: las cadenas Ibérica y Costera Catalana. In: Vera, J.A. (Ed.), Geología de España. Sociedad Geológica de España, Salamanca, Spain. Ministerio de Educación y Ciencia, Instituto Geológico y Minero de España, pp. 602–617 (In Spanish).

Han, X., Shi, D., Lu, X., 2018. Concentration and source of trace metals in street dust from an industrial city in semi-arid area of China. J. Environ. Sci. Manag. 21, 90–99. https://doi.org/10.47125/jesam/2018_1/09.

Hansen, T.W., DeLaRiva, A.T., Challa, S.R., Datye, A., 2013. Sintering of catalytic nanoparticles: particle migration or Ostwald ripening? Acc. Chem. Res. 46 (8), 1720–1730. https://doi.org/10.1021/ar3002427.

Haynes, H.M., Taylor, K.G., Rothwell, J., Byrne, P., 2020. Characterisation of road-dust sediment in urban systems: a review of a global challenge. J. Soils Sediments 20, 4194–4217. https://doi.org/10.1007/s11368-020-02804-y.

Heck, R.M., Farrauto, R.J., 2001. Automobile exhaust catalysts. App. Catal. A Gen. 221, 443–457. https://doi.org/10.1016/S0926-860X(01)00818-3.

Higashi, K., Sonoda, K., Ono, H., Sameshima, S., Hirata, Y., 1999. Synthesis and sintering of rare-earth-doped ceria powder by the oxalate coprecipitation method. J. Mater. Res. 14, 957–967. https://doi.org/10.1557/JMR.1999.0127.

IDESCAT. Institut d'Estadística de Catalunya.2019 https://www.idescat.cat/(accessed 16 August 2022).

2 ICGC. Institut Geològic de Catalunya, Vissir3. http://www.icc.cat/vissir3/(accessed 20 March 2019).

Kitto, E.M., Anderson, D.L., Gordon, G.E., Olmez, I., 1992. Rare earth distributions in catalysts and airborne particles. Environ. Sci. Technol. 26, 1368–1375. https://doi.org/10.1021/es00031a014.

Kulkarni, P., Chellam, S., Fraser, M., 2006. Lanthanum and lanthanides in atmospheric fine particles and their apportionment to refinery and petrochemical operations in Houston, TX. Atmos. Environ. 40, 508–520. https://doi.org/10.1016/j.atmosenv.2005.09.063.

Kulkarni, P., Chellam, S., Fraser, M., 2007. Tracking petroleum refinery emission events using lanthanum and lanthanides as elemental markers for $PM_{2.5}$. Environ. Sci. Technol. 41, 6748–6754. https://doi.org/10.1021/es062888i.

McDonough, W.F., Sun, S.-S., 1995. The composition of the Earth. Chem. Geol. 120, 223–253. https://doi.org/10.1016/0009-2541(94)00140-4.

Meza-Figueroa, D., Pedroza-Montero, M., Barboza-Flores, M., Navarro-Espinoza, S., Ruiz-Torres, R., Robles-Moruá, A., Romero, F., Schiavo, B., González-Grijalva, B., Acosta-Elias, M., Mendoza-Córdova, A., 2021. Identification of refractory zirconia from catalytic convers in dust: an emerging pollutan in urban environments. Sci. Total Environ. 760, 143384 https://doi.org/10.1016/j.scitotenv.2020.143384.

Mikołajczak, P., Borowiak, K., Niedzielski, P., 2017. Phytoextraction of rare earth elements in herbaceous plant species growing close to roads. Environ. Sci. Pollut. Res. 24, 14091–14103. https://doi.org/10.1007/s11356-017-8944-2.

Mleczek, P., Borowiak, K., Budka, A., Niedzielski, P., 2018. Relationship between concentration of rare earth elements in soil and their distribution in plants growing near a frequented road. Environ. Sci. Pollut. Res. 25, 23695–23711. https://doi.org/10.1007/s11356-018-2428-x.

Moreno, T., Karanasiou, A., Amato, F., Leucarelli, F., Nava, S., Calzolai, G., Chiari, M., Coz, E., Aríñano, B., Lumbreras, J., Borge, R., Boldo, E., Linares, C., Alastuey, A., Querol, X., Gibbons, W., 2013. Daily and hourly sourcing of metallic and mineral

dust in urban air contaminated by 2 traffic and coal-burning emissions. Atmos. Environ. 68, 33–44. https://doi.org/10.1016/j.atmosenv.2012.11.037.
Moreno, T., Querol, X., Alastuey, A., de la Rosa, J., Sánchez de la Campa, A., Minguillón, M.C., Pandolfi, M., González-Castanedo, Y., Monfort, E., Gibbons, W., 2010. Variations in vanadium, nickel and lanthanoid element concentrations in urban air. Sci. Total Environ. 408, 4569–4579. https://doi.org/10.1016/j.scitotenv.2010.06.016.
Moreno, T., Querol, X., Alastuey, A., Gibbons, W., 2008a. Identification of FCC refinery atmospheric pollution events using lanthanoid- and valadium- bearting aerosols. Atmos. Environ. 42, 7851–7861. https://doi.org/10.1016/j.atmosenv.2008.07.013.
Moreno, T., Querol, X., Alastuey, A., Pey, P., Cruz Minguillón, M., Pérez, N., Bernabé, R., Blanco, S., Cárdenas, B., Gibbons, W., 2008b. Lanthanoid geochemistry of urban atmospheric particulate matter. Environ. Sci. Technol. 42, 6502–6507. https://doi.org/10.1021/es800786z.
Moreno, T., Querol, X., Castillo, S., Alastuey, A., Cuevas, E., Herrmann, L., Elvira, J., Giboons, W., 2006. Geochemical variations in aeolian mineral particles from the sahara–sahel dust corridor. Chemposphere 65, 261–270. https://doi.org/10.1016/j.chemosphere.2006.02.052.
Morera-Gómez, Y., Alonso-Hernández, C.M., Santamaría, J.M., Elustondo, D., Lasheras, E., Widory, D., 2020. Levels, spatial distribution, risk assessment, and sources of environmental contamination vectored by road dust in Cienfuegos (Cuba) revealed by chemical and C and N stable isotope compositions. Environ. Sci. Pollut. Res. 27, 2184–2196. https://doi.org/10.1007/s11356-019-06783-7.
Najmeddin, A., Keshavarzi, B., Moore, F., Lahijanzadeh, A., 2018. Source apportionment and health risk assessment of potentially toxic elements in road dust from urban industrial areas of Ahvaz megacity, Iran. Environ. Geochem. Health 40, 1187–1208. https://doi.org/10.1007/s10653-017-0035-2.
Navarro-Espinoza, S., Meza-Figueroa, D., Guzmán, R., Duarte-Moller, A., Esparza-Ponce, H., Paz-Moreno, F., González-Grijalva, B., Álvarez-Bajo, O., Schiavo, B., Soto-Puebla, D., Pedroza-Montero, M., 2022. Release of nanoparticles in the environment and catalytic converters ageing. Nanomaterials 11, 3406. https://doi.org/10.3390/nano11123406.
Nolting, R.F., Ramkema, A., Everaats, J.M., 1999. The geochemistry of Cu, Cd, Zn, Ni and Pb in sediment cores from the continental slope of the Banc d'Arguin (Mauritania). Continent. Shelf Res. 19, 665–691. https://doi.org/10.1016/S0278-4343(98)00109-5.
Ogunsola, O.J., Oluwole, A.F., Asubiojo, O.I., Olaniyi, H.B., Akeredolu, F.A., Akanle, O. A., Spyrou, N.M., Ward, N.I., Ruckd, W., 1994. Traffic pollution: preliminary elemental characterisation of roadside dust in Lagos, Nigeria. Sci. Total Environ. 175–184. https://doi.org/10.1016/0048-9697(94)90235-6.
Olmez, I., Gordon, G., 1985. Rare earths: atmospheric signatures for Oil-Fired power plants and refineries. Science 229, 966–968. https://doi.org/10.1126/science.229.4717.966.
Olmez, I., Sheffiel, A., Gordon, G., Houck, J., Critchett, C., Cooper, J., Dzubay, T., Bennet, R., 1988. Compositions of particles from selected sources in Philadelphia for receptor modeling applications. J. Air Waste Manag. Assoc. 38, 1392–1402. https://doi.org/10.1080/08940630.1988.10466479.
Ondov, J.M., Zoller, W.H., Gordon, G.E., 1982. Trace element emissions on aerosols from motor vehicles. Environ. Sci. Technol. 16, 318–328. https://doi.org/10.1021/es00100a004.
Pacyna, J.M., Semb, A., Hanssen, J.E., 1984. Emissions and long-range transport of trace elements in Europe. Tellus B: Chem. Phys. Meteorol. 36, 163–178. https://doi.org/10.3402/tellusb.v36i3.14886.
Pagano, G., Guida, M., Tommasi, F., Oral, R., 2015. Health effects and toxicity mechanisms of rare earth elements—knowledge gaps and research prospects. Ecotoxicol. Environ. Saf. 115, 40–48. https://doi.org/10.1016/j.ecoenv.2015.01.030.
Reche, C., Querol, X., Alastuey, A., Viana, M., Pey, J., Moreno, T., Rodríguez, S., Gonzalez, Y., Fernandez-Camacho, R., Sanchez de la Campa, A., de la Rosa, M., Dall'Osto, A., Prévôt, S., Hueglin, C., Harrison, R., Quincey, M., 2011. New considerations for PM, Black Carbon and particle number concentration for air quality monitoring across different European cities. Atmos. Chem. Pys. 11, 6207–6227. https://doi.org/10.5194/acp-11-6207-2011.
Reddy, B.M., Khan, A., 2005. Nanosized CeO_2–SiO_2, CeO_2–TiO_2, and CeO_2–ZrO_2 mixed oxides: influence of supporting oxide on thermal stability and oxygen storage properties of ceria. Catal. Surv. Asia 9, 155–171. https://doi.org/10.1007/s10563-005-7552-1.
Reimann, C., Caritat, P., 2000. Intrinsic flaws of element enrichment factors (EFs) in environmental geochemistry. Environ. Sci. Technol. 34 (24), 5084–5091. https://doi.org/10.1021/es001339o.
Rudnick, R.L., Gao, S., 2003. The composition of the continental crust. In: Rudnick, R.L. (Ed.), The Crust. Elsevier-Pergamon, Oxford, pp. 1–64. https://doi.org/10.1016/B0-08-043751-6/03016-4.
Sabbioni, E., Pietra, R., Gaglione, P., Vocaturo, G., Colombo, F., Zanoni, M., Rodi, F., 1982. Long-term occupational risk of rare-earth pneumoconiosis: a case report as investigated by neutron activation analysis. Sci. Total Environ. 26, 19–32. https://doi.org/10.1016/0048-9697(82)90093-6.
Sánchez, A.M., Moreno, T., de la Rosa, J., Alastuey, A., Querol, X., 2011. Size distribution and chemical composition of metalliferous stack emissions in the San Roque petroleum refinery complex, southern Spain. J. Hazard Mater. 190, 713–722. https://doi.org/10.1016/j.jhazmat.2011.03.104.
Santanach, P., Casas, J.M., Gratacós, O., Liesa, M., Muñoz, J.A., Sàbat, F., 2011. Variscan and Alpine structure of the Hills of Barcelona: geology in an urban area. J. Iber. Geol. 37, 121–136. https://doi.org/10.5209/rev_JIGE.2011.v37.n2.2.
Shajib, M.T.I., Hansen, H.C.B., Liang, T., Holm, P.E., 2020. Rare earth elements in surface specific urban runoff in Northern Beijing. Sci. Total Environ. 717, 136969 https://doi.org/10.1016/j.scitotenv.2020.136969.
Skublov, S.G., Astaf'ev, B.Y., Marin, Y.B., Gembitskaya, I.M., Levchenkov, O.A., 2009. First find of cerianite in zircons from metasomatites of the Terskii greenstone belt, Baltic shield. Dokl. Earth Sci. 428, 1134. https://doi.org/10.1134/S1028334X09070216.
Taghavi, S.N., Kamani, H., Dehghani, M.H., Nabizadeh, R., Afshari, N., Mahvi, A.M., 2017. Assessment of heavy metals in street dusts of tehran using enrichment factor and geo-accumulation index. Health Scope 8, e57879. https://doi.org/10.5812/jhealthscope.57879.
Taylor, S.R., McLennan, S.M., 1995. The geochemical evolution of the continental crust. Rev. Geophys. 33, 241–265. https://doi.org/10.1029/95RG00262.
Tian, S., Liang, T., Li, K., 2019. Fine road dust contamination in a mining area presents a likely air pollution hotspot and threat to human health. Environ. Int. 128, 201–209. https://doi.org/10.1016/j.envint.2019.04.050.
Trovarelli, A., 1996. Catalytic properties of ceria and CeO_2-containing materials. Catal. Rev. - Sci. Eng. 38, 439–520. https://doi.org/10.1080/01614949608006464.
Ulutaş, K., 2022. Risk assessment and spatial distribution of heavy metal in street dusts in the densely industrialized area. Environ. Monit. Assess. 194, 99. https://doi.org/10.1007/s10661-022-09762-7.
Valdés, A., Pové, M., Munoz, M., Toutain, J., Morata, D., 2013. Geochemical features of aerosols in Santiago de Chile from time series analysis. Environ. Earth Sci. 69, 2073–2090. https://doi.org/10.1007/s12665-013-2415-y.
Varrica, D., Dongarrà, G., Sabatino, G., Monna, F., 2003. Inorganic geo-chemistry of roadway dust from the metropolitan area of Palermo. Italy. Environ. Geol. 44, 222–230. https://doi.org/10.1007/s00254-002-0748-z.
Wang, C., Zhu, W., Wang, Z., Guicherit, R., 2000. Rare earth elements and other metals in atmospheric particulate matter in the western part of The Netherlands. Water Air Soil Pollut. 121, 109–118. https://doi.org/10.1023/A:1005293131518.
WHO, 2016. Ambient Air Pollution: a Global Assessment of Exposure and Burden of Disease. World Health organization, p. 121pp.
Wiseman, C.L.S., Pour, Z.H., Zereini, F., 2016. Platinum group element and cerium concentrations in roadside environments in Toronto, Canada. Chemosphere 145, 61–67. https://doi.org/10.1016/j.chemosphere.2015.11.056.
Yasnygina, T., Rasskazov, S., Markova, M., Zharov, A.E., Malykh, Y., Saranina, E., Fefelov, N., 2015. Trace elements and Sr isotopes in the crude oils from the Sakhalin offshore fields. Russ. J. of Pac. Geol. 9, 109–119. https://doi.org/10.1134/S1819714015020074.
Yongming, H., Peixuan, D., Junji, C., Posmentier, E.S., 2006. Multivariate analysis of heavy metal contamination in urban dusts of Xi'an, Central China. Sci. Total Environ. 355, 176–186. https://doi.org/10.1016/j.scitotenv.2005.02.026.
Yoshida, H., Koide, T., Uemura, T., Kuzuhara, Y., Ohyama, J., Masato Machida, M., 2022. Ce-modified Rh overlayer for a three-way catalytic converter with oxygen storage/release capability. Catal. Today. https://doi.org/10.1016/j.cattod.2022.04.028 (in press).
Zaengle, T.H., Ndayishimiye, A., Tsuji, K., Fan, Z., Bang, S.H., Perini, J., Misture, S.T., Randall, C.A., 2020. Single-step densification of nanocrystalline CeO_2 by the cold sintering process. J. Am. Ceram. Soc. 103, 2979–2985. https://doi.org/10.1111/jace.17003.
Zaitsev, A.N., Chakhmouradian, A.R., Siidra, O.I., Spratt, J., Williams, C.T., Stanley, C.J., Petrov, S.V., Britvin, S.N., Polyakova, E.A., 2011. Fluorine-, yttrium- and lanthanide-rich cerianite-(Ce) from carbonatitic rocks of the Kerimasi volcano and surrounding explosion craters, Gregory Rift, northern Tanzania. Miner. Mag. 75, 2813–2822. https://doi.org/10.1180/minmag.2011.075.6.2813.
Zhang, L., Zaho, Y., Jin, Z., Bai, G., Yang, L., 2009. Geochemical characteristics of rare earth elements in petroleum and their responses to mantle-derived fluid: an example from the Dongying Depression, East China. Energy Explor 27, 47–68. https://doi.org/10.1260/014459809788708200.

Further reading

Ahmed, F., Bibi, M.H., Ishiga, H., 2007. Environmental assessment of Dhaka City (Bangladesh) based on trace metal contents in road dusts. Environ. Geol. 51, 975–985. https://doi.org/10.1007/s00254-006-0367-1.
Angelone, M., Spaziani, F., Cremisini, C., Salluzzo, A., 2007. In: Morrison, G.M., Rauch, S. (Eds.), Highway and Urban Environment. Alliance for Global Sustainability Bookseries, 12. Springer, Dordrecht, pp. 271–281. https://doi.org/10.1007/978-1-4020-6010-6_25.
Fedotov, P.S., Ermolin, M.S., Karandashev, V.K., Ladonin, D.V., 2014. Characterization of size, morphology and elemental composition of nano-, submicron, and micron particles of street dust separated using field-flow fractionation in a rotating coiled column. Talanta 130, 1–7. https://doi.org/10.1016/j.talanta.2014.06.040.
Long, Y., Chi, G., Qing, H., Dai, T., Wu, Q., 2011. Sources of polycyclic aromatic hydrocarbons in street dust from the Chang-Zhu-Tan Region, Hunan, China. J. Environ. Prot. Sci. 2, 1331–1340. https://doi.org/10.4236/jep.2011.210153.
Nory, R.M., Figueiredo, A.M.G., 2019. Rare earth elements, U and Th in tunnel dusts of São Paulo city, Brazil. Braz. J. Radiat. Sci. 7, 1–9. https://doi.org/10.15392/bjrs.v7i2A.569.
Sun, G., Li, Z., Liu, T., Chen, J., Wu, T., Feng, X., 2017. Rare earth elements in street dust and associated health risk in a municipal industrial base of central China. Environ. Geochem. Health 39, 1469–1486. https://doi.org/10.1007/s10653-017-9982-x.
Yang, Z., Ruilian, Y., Gongren, H., Xiaohui, L., Xianrong, L., 2017. Characteristics and environmental significance of rare earth elements in $PM_{2.5}$ of Nanchang, China. J. Rare Earths 35, 98–106. https://doi.org/10.1016/S1002-0721(16)60179-5.